

**UCSF**

**UC San Francisco Electronic Theses and Dissertations**

**Title**

Improving Quantification of Prostate-Specific Membrane Antigen (PSMA) - Positron Emission Tomography (PET) Clinical Data

**Permalink**

<https://escholarship.org/uc/item/1bz5t8vg>

**Author**

Zhang, Ningjing

**Publication Date**

2023

Peer reviewed|Thesis/dissertation

Improving Quantification of Prostate-Specific Membrane Antigen (PSMA) - Positron Emission Tomography (PET) Clinical Data


by  
Ningjing Zhang

THESIS  
Submitted in partial satisfaction of the requirements for degree of  
MASTER OF SCIENCE

in  
Biomedical Imaging


in the  
GRADUATE DIVISION  
of the  
UNIVERSITY OF CALIFORNIA, SAN FRANCISCO

Approved:

DocuSigned by:  
  
1644A2CD853841E... Peder Larson  
Chair

DocuSigned by:  
  
Thomas Hope

DocuSigned by:  
  
Julian Hong

DocuSigned by:  
  
070ED2AA0DC3441... Susan Noworolski

Committee Members



## **DEDICATIONS AND ACKNOWLEDGEMENTS**

I would like to express my heartfelt gratitude to the individuals and institutions that have contributed to the successful completion of this study. Their unwavering support, guidance, and expertise have been invaluable throughout this journey. First and foremost, I am immensely thankful to my thesis adviser, Dr. Peder Larson. His profound knowledge, dedication, and mentorship have been instrumental in shaping the direction of this research. I extend my sincere appreciation to my co-mentor, Dr. Abhejit Rajagopal, from the Department of Radiology & Biomedical Imaging at the University of California San Francisco. His collaborative spirit, expertise, and willingness to share his insights have greatly contributed to the depth and quality of this study. Working under his guidance has been both enlightening and motivating. I am deeply indebted to Dr. Tom Hope and Dr. Julian Hong. Their constructive feedback, critical insights, and encouragement have played a pivotal role in refining the scope and methodology of this research. Additionally, I want to thank Dr. Susan Noworolski for providing me feedbacks on revising the thesis, and Dr. Courtney Lawhn Heath for her advice and support during this thesis. I also want to express my gratitude to Dr. Surekha Yadav and Fayyaz Ahamed for their invaluable contribution in providing me with additional datasets for training purposes. In addition to the forementioned acknowledgments, I would also like to extend my heartfelt appreciation to Dr. Elizabeth Smith. My project stands as a direct result of building upon the foundational work and insights that she has contributed to this field. Her innovative ideas and pioneering contributions have served as a guiding light throughout my research journey. The depth of understanding I gained from studying her work has been an essential cornerstone in shaping the direction and methodology of my own project.

I would also like to extend my sincere appreciation to everyone in Dr. Michael Evans' lab for their invaluable contribution to my journey. Their shared expertise and generosity in providing me with a solid background knowledge have been instrumental in shaping the foundation of my research. The collaborative atmosphere of Dr. Evans' lab has been a source of inspiration and a driving force behind my commitment to working on this project. I am deeply grateful for the profound impact they have had on my academic and personal growth.

On a personal note, I want to express my profound gratitude to my friends, family, significant other and my cat JoJo. Their unwavering support, unconditional love, and constant encouragement have been my pillars of strength throughout this endeavor. Their belief in my abilities have been a driving force behind my achievements.

Improving Quantification of Prostate-Specific Membrane Antigen (PSMA) - Positron Emission  
Tomography (PET) Clinical Data

Ningjing Zhang

**ABSTRACT**

Prostate cancer is a significant global health concern, ranking as the second most diagnosed cancer and fifth leading cause of cancer-related deaths in men worldwide. Prostate-specific membrane antigen (PSMA)-targeted positron emission tomography (PET) is used for staging, especially in intermediate to high-risk cases and biochemical recurrence, offering superior sensitivity and specificity compared to conventional methods. Despite advancements, the analysis of PSMA-PET data remains largely manual, prompting the need for computer-aided diagnosis using machine learning or deep learning to enhance efficiency and consistency. Some previous works have been done to develop a prediction model based on deep neural network (DNN), however it failed in prediction of high-volume disease cases. In this project, I hypothesized that refined lesion annotation and specialized batching strategies can enhance algorithm performance, leading to improved segmentation accuracy, and SUV measurements. The successful implantation of better contour of the lesion was done by a clinical fixed-threshold method. The results suggested the refined lesion annotations significantly impacted the SUV-mean values in lesions and will further affect the result of DNN training.

**Keywords:** prostate-specific membrane antigen (PSMA), positron emission tomography (PET) Imaging, lesion segmentation

## Table of Contents

1. Introduction.....	1
2. Methods.....	5
3. Results.....	9
4. Discussion.....	13
5. Conclusion.....	15
References.....	16

## List of Figures

Figure 1.1 General workflow.....	4
Figure 2.1 Example of previous annotations.....	6
Figure 2.2 Workflow of generating better ground truth .....	6
Figure 2.3 Workflow of generating better ground truth .....	7
Figure 3.1. Non-ideal Result from histogram-based method.....	9
Figure 3.2: Example of the comparison between the mask generated by previous annotation and after the thresholding.....	10
Figure 3.3: Scatter plot of SUV-max and SUV-mean distribution of lesions before and after contouring the ground truth.....	11
Figure 3.4: Histogram of SUV-max and SUV-mean distribution of lesions before and after contouring the ground truth.....	11



## List of Tables

Table 1.1 Common PSMA-PET tracers in clinical use.....	2
Table 3.1 KL divergence, MI results between two masks .....	12

## **List of Abbreviations**

AMI: adjusted mutual information

CAD: computer-aided diagnosis

CT: computerized tomography

DICOM: digital imaging and communications in medicine

DNN: deep neural network

HDF5: Hierarchical Data Format version 5

KL: Kullback–Leibler

MIP: Maximum intensity projection

ML: machine learning

NIfTI: Neuroimaging informatics technology initiative

NMI: normalized mutual information

PET: positron emission tomography

PSMA: prostate-specific membrane antigen

ROI: region of interest

VOI: Volume of Interest

## **1.Introduction**

### **1.1 Prostate Cancer and PSMA-targeted PET**

Prostate cancer is a major health issue that affects men globally. It is the second most diagnosed cancer and the fifth leading cause of cancer-related deaths in men worldwide [1]. Globally, more than 1.4 million new prostate cancer cases were diagnosed, and more than 375 thousand related deaths were reported in 2020 [1]. According to different stages of prostate cancer (localized, locally advanced, and metastatic disease), different treatment should be administrated to reduce both under- and over-treatment [2]. However, the choice of treatment can be challenging due to the heterogeneity of the disease [2]. Thus, it is essential to have accurate diagnosis. Prostate-specific membrane antigen (PSMA), a transmembrane protein that is highly expressed in prostate cancer cells, plays a critical role in positron emission tomography (PET) imaging [3]. PSMA-PET tracers are usually used for staging intermediate, high-risk and very high-risk prostate cancer patients and for patients with biochemical recurrence [4]. The advantages of PSMA-PET over conventional imaging techniques such as CT and bone scan include higher sensitivity and specificity, improved detection of small lesions, and better differentiation between benign and malignant lesions [4]. PSMA-PET also allows for more accurate localization of lesions, which can aid in treatment planning and monitoring [4].

PSMA-PET tracers have a relatively short history, with the first molecular imaging agent for prostate cancer, In-capromab pendetide (ProstaScint), being approved by the FDA in 1996 [5]. However, this tracer had limited performance due to its targeting of only dying or dead cells [5]. The first antibodies to the extracellular domain of PSMA were developed in 1997, enabling studies of PSMA in viable cells [5]. Since then, PSMA-PET has been

investigated as a biomarker for selecting patients for PSMA-directed therapy, including PSMA-11, PSMA-617, DCFPyL, and PSMA-1007 (**Table 1.1**) [5,6].

**Table 1.1:** Common PSMA-PET Tracers in clinical use

Tracers	Isotope	Application
PSMA-11	$^{68}\text{Ga}$	Diagnostics
PSMA-617	$^{68}\text{Ga}$ , $^{177}\text{Lu}$ , $^{225}\text{Ac}$	Theranostics
DCFPyL	$^{18}\text{F}$	Diagnostics
PSMA-1007	$^{18}\text{F}$	Diagnostics

Among these, PSMA-11 is the most-studied PSMA-targeted PET tracers, with its initial report dating back to 2007 [7]. Subsequent preclinical evaluations in 2012 were followed by the first clinical reports in 2012 [8, 9]. Notably, on December 1, 2020, PSMA-11 received FDA approval for both New Drug Applications (NDAs) submitted by UCSF and UCLA [10]. This marked a significant milestone, making PSMA-11 the first Gallium-68-labeled radiopharmaceutical approved for PET imaging of PSMA-positive prostate cancer. Other common tracers have expanded applications, including both diagnostic (using Ga-68 and F-18) and therapeutic (using Lu-177 and Ac-225) purposes [6]. And so far, most of PSMA-PET image data is analyzed manually by the specialists in nuclear medicine based on their experience, which is a time-consuming and error-prone process, leading to a high number of inter- and intra-observer variability [11]. Thus, there is a need to use computer-aided diagnosis (CAD) via machine learning (ML) or deep learning (DL) tools to automate and standardize repetitive tasks currently performed by physicians, freeing up their time to focus on more complex patient care, and thus reduce costs and improve health outcomes for underserved populations.

## 1.2 Hypothesis and Goals

Although there are some ML algorithms which are able to detect and characterize prostate cancer lesions, they still have some limitations due to data inconsistency, overfitting, and generalization issues [11]. Therefore, there is a need for further research and validation studies to establish the clinical utility of ML in PSMA-PET imaging and to ensure the effective implementation of these techniques in clinical practice. This project aims to improve deep DL models which can extract relevant features from clinical Ga-68-PSMA-11-PET reconstructions and perform good segmentation so that the PSMA-PET positive volume and standardized uptake values (SUV, including SUV-max and SUV-mean) in bone, liver, lymph node, and other lesions can be calculated. The hypothesis was that enhancing the accuracy of lesion annotation will lead to improved algorithm performance. This can be achieved by employing more effective contouring techniques to minimize background information within the region of interest (ROI). To test this, the experiment previously conducted by Dr. Smith should be replicated, with a focus on quantifying potential enhancements in segmentation accuracy. Additionally, the effects of the refined segmentation on SUV (Standardized Uptake Value) measurements and patient survival rates should be assessed through sensitivity analysis. If successful, the utilization of ML techniques in PSMA-PET imaging has the potential to significantly improve the accuracy of tumor volume estimation and enhance treatment planning for prostate cancer patients. By providing a quantitative PSMA-PET biomarker report, this tool can aid radiologists and nuclear medicine specialists in making informed decisions, ultimately leading to more effective and personalized care. This will benefit the development of tailored prostate cancer research and improve patient outcomes.

### 1.3 Previous Work

Some previous works have been done on this project by Dr. Elizabeth Smith. There was a previous prediction model based on 3D U-Net which was trained on 250 whole-body Ga-68-PSMA-11 positive PET scans with annotations and generated predictions for the SUV-max and SUV-mean values. The previous prediction model works well on the low-volume diseases. However, it fails on the high-volume ones because the current ground truth is not the actual ground truth. More specifically, the ground truth we have now is the annotations from the radiologists which are bigger than the lesion. This leads to the inaccurate tumor volume estimation after segmentation which results in an inaccurate prediction. Therefore, we need to refine the segmentation neural networks to get more accurate lesions regions for better tumor volume estimation and have more high-volume datasets in the training.

Furthermore, the choice of right batch size is also important for optimizing the training because it will affect the generalization performance and the accuracy of the gradient estimates used to update the model parameters. **Fig.1.1** is the general workflow of the project, and in

project, and in

this project, I

focused on the

improvement of

DNN

performance via

better ground truth.

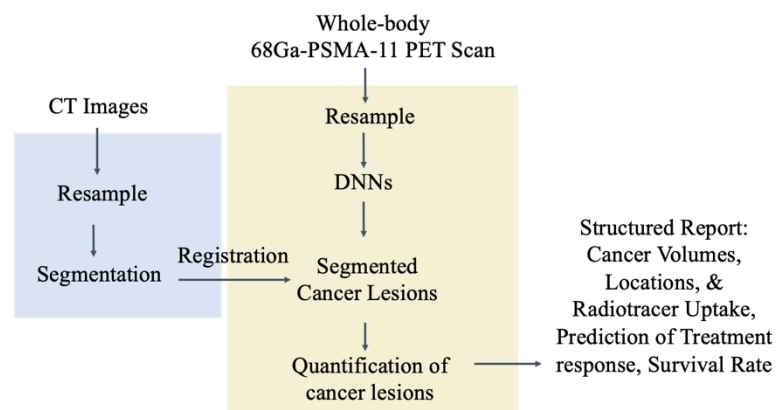


**Figure 1.1:** General workflow

## 2 Methods

### 2.1 Datasets

The datasets were from UCSF Medical Center. The datasets employed in this study consist of a meticulously curated collection of 250 scans depicting PSMA-positive cases. All the patient personal information was removed, and a new ID was generated for each of the patients. The selection of new scans was conducted using a stratified sampling approach, aiming to optimize the incorporation of various factors that contribute to fluctuations in image quality and the distribution of radiotracers. Dr. Thomas Hope meticulously annotated approximately 1,000 lesions within the dataset. Additionally, a comprehensive analysis of thousands of radiology reports was undertaken to identify around 70 instances of PSMA negative scans. This dataset serves as a robust foundation for training and evaluating models, encompassing a diverse range of scenarios and tumor volume distributions.

### 2.2 Better Ground Truth Generation

As mentioned before, the previous annotations did not provide the best contour for the lesions. One example is shown in **Fig 2.1**. The lesion was small (the bright spot inside the red box in the first figure), while the annotation was much larger as shown in the second figure with the white circle. The histogram plot inside this ROI also demonstrated that there were plenty of background information in this annotation. Therefore, it led to inaccurate SUV-mean and total tumor volume estimation.

To mitigate this problem, a histogram-based method provided by Burger et al. was investigated in generating new masks [12]. According to Burger et al, the background subtracted lesion (BSL) activity can be calculated by a new histogram-based method to determine the tumor activity by subtraction of a Gaussian fit over the peak of the histogram from the volume of interest (VOI)

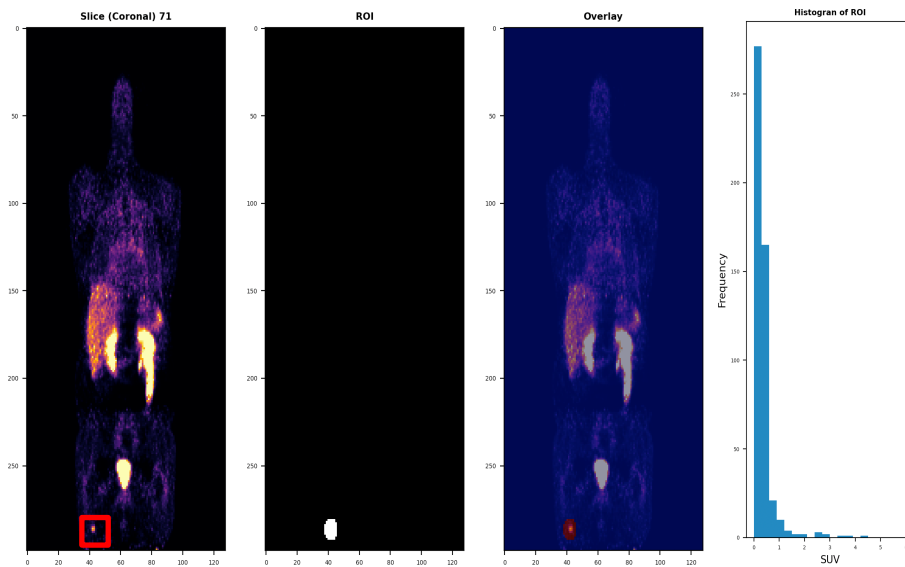


**Figure 2.1:** Example of previous annotations. The first column (left) is a clinical PSMA-PET image. Red box indicated the location of the lesion. The second column is the mask generated for the lesion. The third column is the overlay of the mask and the PET image. The fourth column is a histogram indicating the majority of SUV values came from the background information.

surrounding the tumor (**Fig 2.2**). The mean background activity of the surrounding tissue,  $SUV_{BG}$ , was estimated by the mode of the histogram [12].

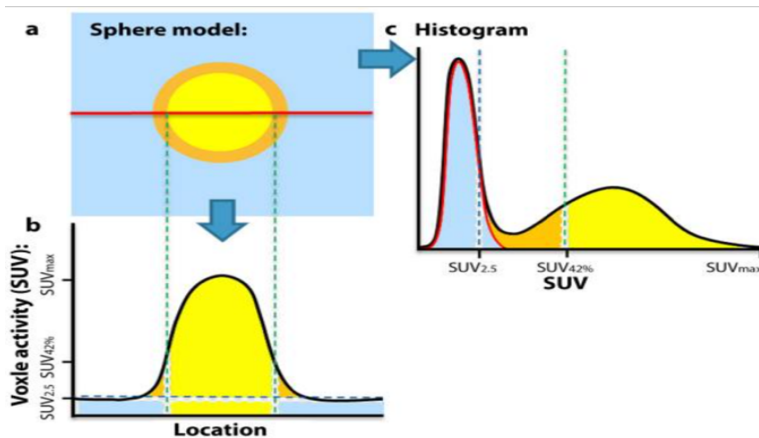


**Figure 2.2:** Illustration of a sphere model with a yellow lesion and spillover (orange) in background activity. The background activity should be the blue area under the curve, and the true volume should be the combination of orange and yellow area.

Another approach to improve the annotation was suggested by Dr. Hope, which is a common clinical fixed-threshold method (**Fig 2.3**).

First, from each of the previous annotation files, the exam ID was extracted and



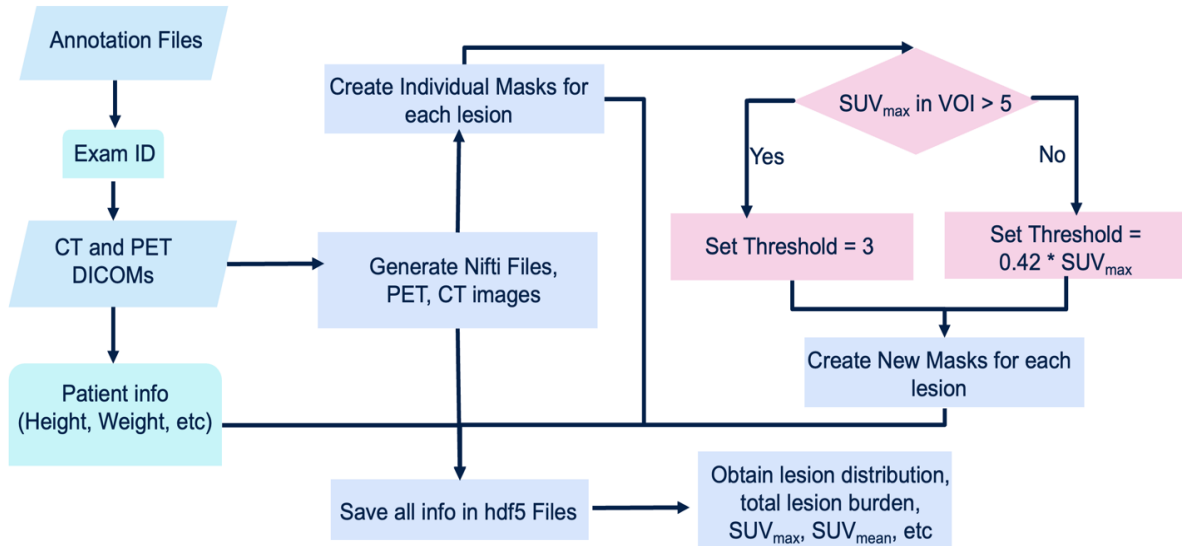


**Figure 2.3:** Workflow of generating better ground truth

used to locate the corresponding computerized tomography (CT) and PET digital imaging and communications in medicine (DICOM) files. Some patient specific information was extracted from DICOM files such as patient weight and height. Then Neuroimaging informatics technology initiative (NIFTI) files were generated separately, and the PET and CT images were stored as a 3D array. By combining the information in those images and previous annotation files, individual masks for each lesion in each patient was created. Then the SUV-max values were extracted from those ROIs selected by the original mask. If the SUV-max was greater than 5, the threshold was set to be three, otherwise the threshold was set to be 42% of the SUV-max. After thresholding, the new masks were generated. Finally, the specific patient info (including exam ID, patient height, patient weight), the old masks, the new masks, PET and CT images were stored in Hierarchical Data Format version 5 (HDF5) file, which was used to obtain useful information such as total lesion volume, SUV-mean values in each lesions to help improve the training strategy.

To better quantify the difference between the distribution of SUV-mean values between two masks, after the new masks were generated, Kullback-Leibler divergence (KL divergence) was

calculated. KL divergence serves as a pivotal measure to gauge the information loss when approximating one distribution with another [13]. Adjusted mutual information (AMI) and normalized mutual information (NMI) were also computed both between the mask 1 itself and between mask 1 and mask 2. AMI is a measure that quantifies the agreement between two clustering assignments while considering chance agreement and NMI evaluates clustering quality by normalizing the Mutual Information score by the entropy of the individual clusters, which provides a measure of the proportion of information shared between the cluster assignments compared to the information in each individual clustering [14,15]. They play a crucial role in accessing the quality of clustering results and can guide the DNN training and hyperparameter tuning.

### 3. Results

#### 3.1 Updated Ground Truth

The results from the histogram-based method were shown in **Fig 3.1**. The results were not ideal as the Gaussian fit did not fit the background pixels very well, which led to inaccurate tumor volume estimation after subtracting the area under the Gaussian fit.

However, the fixed-threshold method provided a better improvement visually. As shown in **Fig 3.2**, in the first maximum intensity projection (MIP) image (top), the patient had two lesions, and in the second image which only contained the previous mask area of the MIP, there were lots of background information. And as indicated in the second image, the masks covered an area larger than the actual lesion. After thresholding, the masks were significantly decreased and were closer

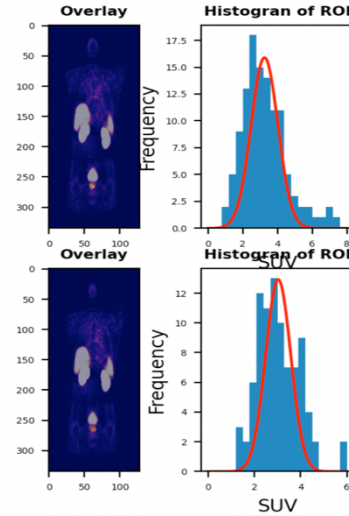


**Figure 3.1:** Non-ideal Result from histogram-based method

to the actual lesion size. The improvement on the fit of the lesion was also confirmed in the scatter plot which compared the distribution of the SUV-max and SUV-mean between the original mask (mask1) and updated mask (mask2) (**Fig 3.3**). Similarly, from the histogram, the distribution of the SUV-mean has significantly changed, as lower SUV-mean values have shifted towards higher values (**Fig 3.4**). Both **Fig 3.3** and **Fig 3.4** indicated that there were no significant change in SUV-max, while an increase in SUV-mean, indicating a better estimate of the lesion voxels.

The results from KL divergence, AMI and NMI also suggested that there was a significant difference between two masks (**Table 3.1**). KL divergence between two masks was 1.01, indicating the two distributions of masks had nonnegligible difference. The AMI score decreased from 1.0 to 0.42 and NMI score decreased from 1.0 to 0.73, both indicating there were some

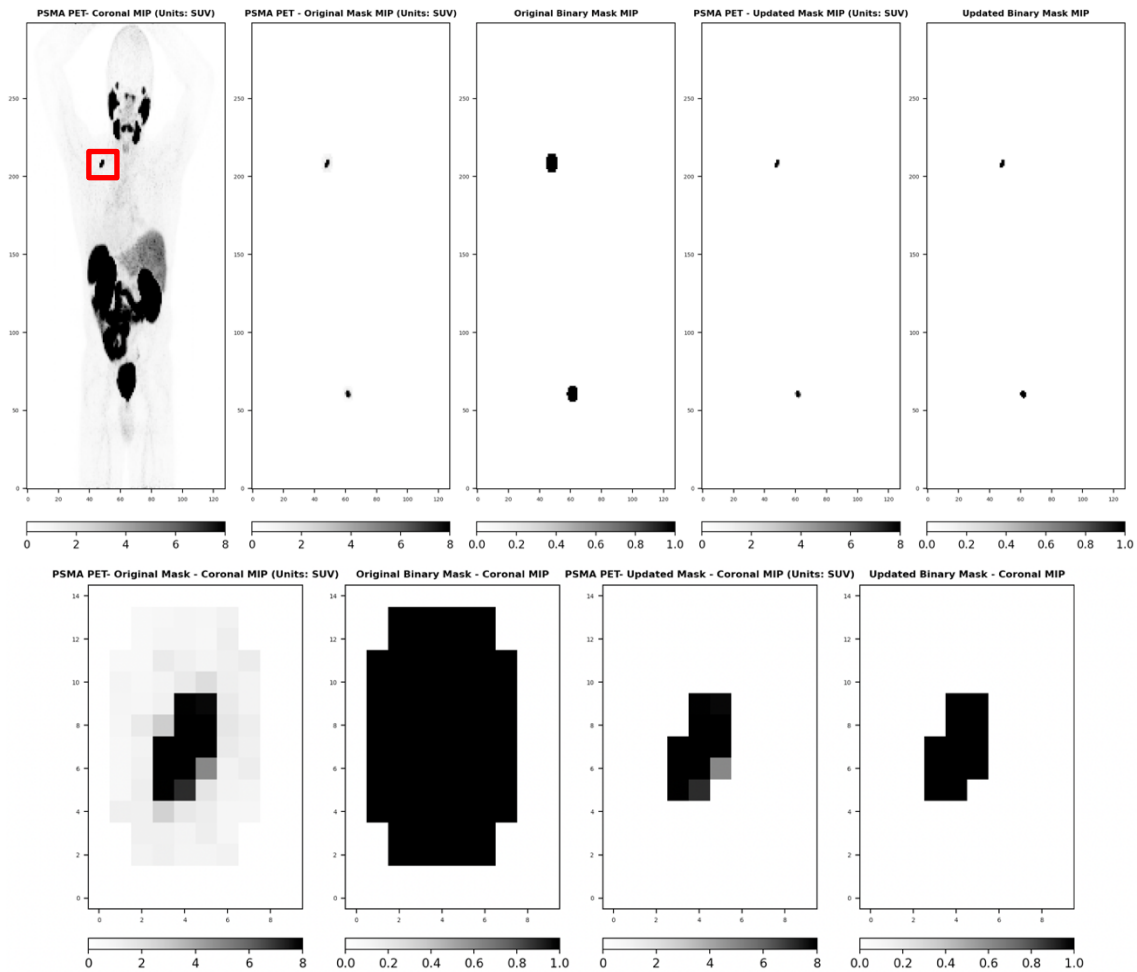


**Figure 3.2:** Example of the comparison between the mask generated by previous annotation and after the thresholding. The bottom row was a zoom-in version of one of the lesions inside the red box shown in the first figure, from which the background information was largely reduced.

similarities between two clusters of masks, but also, they separated certain instances into distinct groups that differ between two masks.

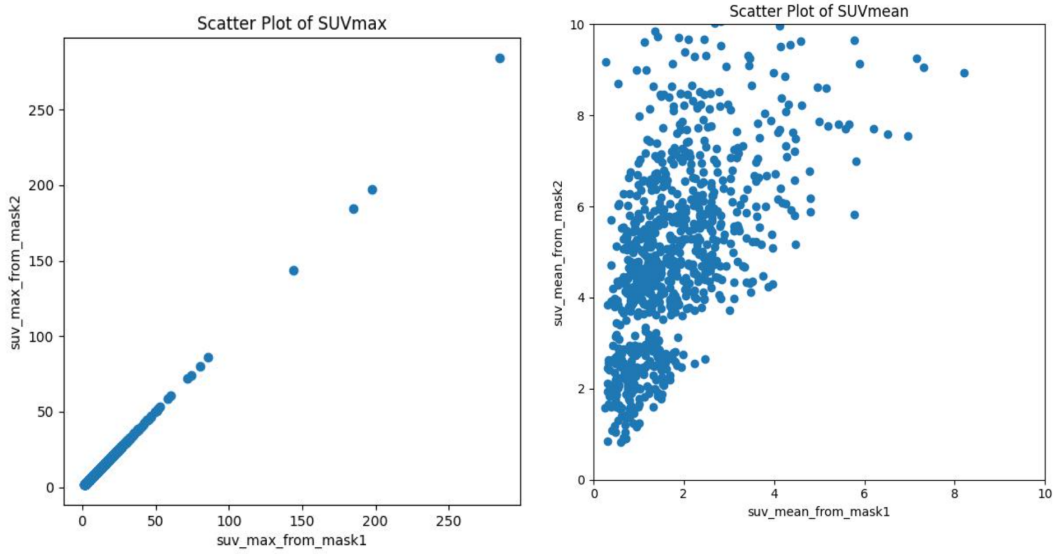


**Figure 3.3:** Scatter plot of SUV-max and SUV-mean distribution of lesions before and after contouring the ground truth

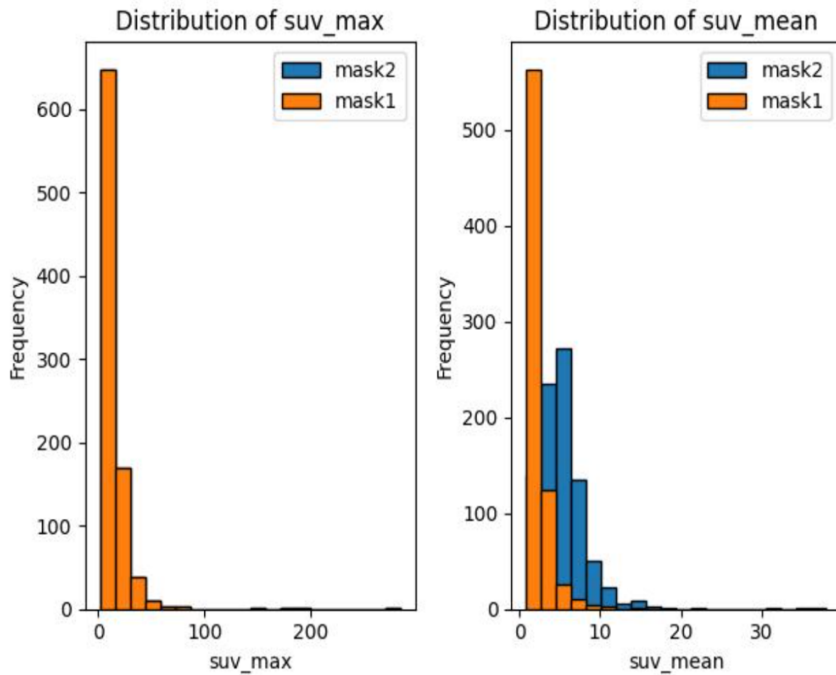


**Figure 3.4:** Histogram of SUV-max and SUV-mean distribution of lesions before and after contouring the ground truth

**Table 3.1** KL divergence, MI results between two masks

	<b>KL Divergence</b>	<b>Adjusted MI</b>	<b>Normalized MI</b>
<b>mask1 to mask 1</b>	<b>N.A.</b>	<b>1.0</b>	<b>1.0</b>
<b>mask1 to mask 2</b>	<b>1.01</b>	<b>0.42</b>	<b>0.73</b>

#### 4. Discussion

This project demonstrated that the better mask contouring algorithms would have an impact on the SUV-mean value in the annotations, which would affect the DNN segmentation accuracy as well as the correlation between SUVmean and patient survival rate. In the quantification of two distribution of the masks, a KL divergence of 1.01 highlights differences in SUV-mean distributions between masks; an AMI score of 0.43 suggests moderate agreement in clustering, while an NMI score of 0.73 indicates substantial normalized agreement. Using these insights can help to guide model training: emphasize distinct and shared patterns, prioritize important features, apply regularization, and validate against ground truth [16]. These values can help establish a balanced model that captures both unique and common information present in the dataset [16].

Admittedly, there are some limitations in this study. First of all, the updated ground truth was generated by a simple thresholding method, which is reported to be very dependent on the signal to noise ratio, tumor to background ratio and the size of the tumor [17]. There might be some better contouring algorithms for this task. There are some literatures introduced how to use dynamic PET threshold to get more accurate SUV-max, SUV-mean measurements from the crude manual annotations generated by radiologists [18,19]. Erdi et al [18] proposed an iterative threshold method in which the optimal thresholds, specific to volume-to-signal-to-background ratios, were fitted using an exponential decay function based on a phantom [18]. Notably, the researchers suggested a fixed threshold (e.g., 42%) for volumes >4 mL due to reduced sensitivity to partial volume effects, while smaller volumes exhibited increased optimal thresholds as lower signal-to-background ratios led to edge-blurring from background activity [18]. Bilger et al [19] also proposed a new

segmentation technique based on adapting a fit function to the soft tissue peak of the histogram in VOI, and they enhanced the method's robustness by introducing an estimated lung position for patient contour finding and lung segmentation. Therefore, in the future research, a more robust contouring algorithm should be investigated for application of more general datasets. Furthermore, it is important to acknowledge that the dataset used in this study remains limited in size and lacks the diversity of multi-center image data.

To address these limitations, future research endeavors could focus on implementing different threshold methods to generate better contoured ground truth and expanding the dataset by incorporating a larger variety of images. This extension would contribute to a more comprehensive validation of the deep neural network model's performance and generalizability. Moreover, the correlation between SUV-mean and clinical data such as patient survival rate can be further evaluated to demonstrate that the improvement in the lesion contouring can lead to more predictive clinical results.



## **5. Conclusion**

In conclusion, a more effective methodology has been devised for the representation and post-processing of physician-annotated lesions in PSMA-PET imaging. The study has highlighted the substantial impact of the chosen contouring algorithm on the calculation of SUV-mean. Notably, the clinical fixed-threshold technique showcased superior performance compared to the histogram-fitting approach. These findings collectively underscore the critical importance of precise lesion annotation and appropriate algorithm selection in the accurate determination of SUV-mean values within PSMA-PET scans.

## References

- [1] L. Wang *et al.*, “Prostate cancer incidence and mortality: Global status and temporal trends in 89 countries from 2000 to 2019,” *Frontiers in Public Health*, vol. 10, 2022.  
doi:10.3389/fpubh.2022.811044
- [2] M. Sekhoacha *et al.*, “Prostate cancer review: Genetics, diagnosis, treatment options, and alternative approaches,” *Molecules*, vol. 27, no. 17, p. 5730, 2022.  
doi:10.3390/molecules27175730
- [3] W. P. Fendler *et al.*, “Assessment of Ga-68-PSMA-11 pet accuracy in localizing recurrent prostate cancer,” *JAMA Oncology*, vol. 5, no. 6, p. 856, 2019.  
doi:10.1001/jamaoncol.2019.0096
- [4] I. Tsehelidis and A. Vrachimis, “PSMA-PET in Imaging prostate cancer,” *Frontiers in Oncology*, vol. 12, 2022. doi:10.3389/fonc.2022.831429
- [5] A. K. Miyahira and H. R. Soule, “The history of prostate-specific membrane antigen as a theranostic target in prostate cancer: The cornerstone role of the Prostate Cancer Foundation,” *Journal of Nuclear Medicine*, vol. 63, no. 3, pp. 331–338, 2021.  
doi:10.2967/jnumed.121.262997
- [6] A. R. Lisney *et al.*, “The role of PSMA-PET/CT in the primary diagnosis and follow-up of prostate cancer—A practical clinical review,” *Cancers*, vol. 14, no. 15, p. 3638, 2022.  
doi:10.3390/cancers14153638

- [7] A. P. Kozikowski et al., “Design of remarkably simple, yet potent urea-based inhibitors of glutamate carboxypeptidase II (naaladase),” *Journal of Medicinal Chemistry*, vol. 44, no. 3, pp. 298–301, 2001. doi:10.1021/jm000406m
- [8] M. Eder et al., “Ga-68-complex lipophilicity and the targeting property of a urea-based PSMA inhibitor for PET imaging,” *Bioconjugate Chemistry*, vol. 23, no. 4, pp. 688–697, 2012. doi:10.1021/bc200279b
- [9] A. Afshar-Oromieh, U. Haberkorn, M. Eder, M. Eisenhut, and CM. Zechmann, “[Ga-68]gallium-labelled PSMA ligand as superior pet tracer for the diagnosis of prostate cancer: Comparison with 18F-fech,” *European Journal of Nuclear Medicine and Molecular Imaging*, vol. 39, no. 6, pp. 1085–1086, 2012. doi:10.1007/s00259-012-2069-0
- [10] G. Carlucci et al., “Ga-68-PSMA-11 NDA approval: A novel and successful Academic Partnership,” *Journal of Nuclear Medicine*, vol. 62, no. 2, pp. 149–155, 2020. doi:10.2967/jnumed.120.260455
- [11] A. Erle *et al.*, “Evaluating a machine learning tool for the classification of pathological uptake in whole-body PSMA-PET-CT scans,” *Tomography*, vol. 7, no. 3, pp. 301–312, 2021. doi:10.3390/tomography7030027
- [12] I. A. Burger *et al.* “PET quantification with a histogram derived total activity metric: superior quantitative consistency compared to total lesion glycolysis with absolute or relative SUV thresholds in phantoms and lung cancer patients.” *Nuclear medicine and biology* vol. 41,5 (2014): 410-8. doi:10.1016/j.nucmedbio.2014.02.006

- [13] J.M. Joyce., Kullback-Leibler Divergence. In: Lovric, M. (eds) International Encyclopedia of Statistical Science. Springer, Berlin, Heidelberg. 2011. doi:10.1007/978-3-642-04898-2\_327
- [14] N.X. Vinh, J. Epps, and J. Bailey, "Information Theoretic Measures for Clusterings Comparison: Variants, Properties, Normalization and Correction for Chance," *JMLR*, vol. 11, no.95, pp.2837–2854, 2010.
- [15] T. Kvålseth, "On normalized mutual information: Measure derivations and properties," *Entropy*, vol. 19, no. 11, p. 631, 2017. doi:10.3390/e19110631
- [16] R. Z. Nasab *et al.* "Deep Learning in Spatially Resolved Transcriptomics: A Comprehensive Technical View." *arXiv:2210.04453*
- [17] T. Mahbubunnabi, "Intensity threshold based solid tumour segmentation method for Positron Emission Tomography (PET) images: A review." *Heliyon* vol. 6, 10 e05267. 27 Oct.2020, doi:10.1016/j.heliyon.2020.e05267
- [18] Y. E. Erdi, O. Mawlawi, S. M. Larson, M. Imbriaco, H. Yeung, R. Finn, and J. L. Humm, "Segmentation of lung lesion volume by adaptive positron emission tomography image thresholding," *Cancer*, vol. 80, no. S12, pp. 2505–2509, 1997.
- [19] K. Bilger, J. Kupferschlager, W. Muller-Schauenburg, F. Nusslin and R. Bares, "Threshold calculation for segmented attenuation correction in PET with histogram fitting," *IEEE*

*Transactions on Nuclear Science*, vol. 48, no. 1, pp. 43-50, Feb 2001, doi:

10.1109/23.910831.

## Publishing Agreement

It is the policy of the University to encourage open access and broad distribution of all theses, dissertations, and manuscripts. The Graduate Division will facilitate the distribution of UCSF theses, dissertations, and manuscripts to the UCSF Library for open access and distribution. UCSF will make such theses, dissertations, and manuscripts accessible to the public and will take reasonable steps to preserve these works in perpetuity.

I hereby grant the non-exclusive, perpetual right to The Regents of the University of California to reproduce, publicly display, distribute, preserve, and publish copies of my thesis, dissertation, or manuscript in any form or media, now existing or later derived, including access online for teaching, research, and public service purposes.

DocuSigned by:

*Mingjing Zhang*

C077CBA9EA104ED...

Author Signature

8/29/2023

Date